The *Mycobacterium tuberculosis* Virulence Factor Trehalose Dimycolate Imparts Desiccation Resistance to Model Mycobacterial Membranes

Christopher W. Harland,* David Rabuka,† Carolyn R. Bertozzi,†‡§¶ and Raghuveer Parthasarathy*
*Department of Physics and Materials Science Institute, University of Oregon, Eugene, Oregon 94703; †Department of Chemistry, University of California, Berkeley, California 94720; ‡Department of Molecular and Cell Biology, University of California, Berkeley, California 94720; §Physical Bioscience and Materials Science Divisions, Lawrence Berkeley National Laboratory, Berkeley, California 94720; and ¶Howard Hughes Medical Institute, University of California, Berkeley, California 94720

ABSTRACT Mycobacteria, including persistent pathogens like *Mycobacterium tuberculosis*, have an unusual membrane structure in which, outside the plasma membrane, a nonfluid hydrophobic fatty acid layer supports a fluid monolayer rich in glycolipids such as trehalose 6,6′-dimycolate (TDM; cord factor). Given the abilities of mycobacteria to survive desiccation and trehalose in solution to protect biomolecules and whole organisms during freezing, drying, and other stresses, we hypothesized that TDM alone may suffice to confer dehydration resistance to the membranes of which it is a constituent. We devised an experimental model that mimics the structure of mycobacterial envelopes in which an immobile hydrophobic layer supports a TDM-rich, two-dimensionally fluid leaflet. We have found that TDM monolayers, in stark contrast to phospholipid membranes, can be dehydrated and rehydrated without loss of integrity, as assessed by fluidity and protein binding. Strikingly, this protection from dehydration extends to TDM-phospholipid mixtures with as little as 25 mol % TDM. The dependence of the recovery of membrane mobility upon rehydration on TDM fraction shows a functional form indicative of spatial percolation, implying that the connectivity of TDM plays a crucial role in membrane preservation. Our observations are the first reported instance of dehydration resistance provided by a membrane glycolipid.

INTRODUCTION

The resurgence of tuberculosis in the developed world and its continued persistence in the developing world are well-known public health concerns. Roughly one third of the human population is infected with *Mycobacterium tuberculosis* (MTb), and nearly two million people die each year as a result (1–3). The biophysical properties of the bacterium are suspected to play a key role in its persistence. All the mycobacteria, including MTb, have a dense outer envelope consisting of large fatty acids whose structure confers considerable impermeability to antibiotic agents as well as, for certain pathogens, biochemical means of manipulating host immune responses (4–6). Mycobacteria also have a well-known (7–9) ability to withstand dry environments. *M. tuberculosis* and *M. leprae*, for example, can survive periods of desiccation lasting several months (10–13). Despite the importance of the mycobacteria, the molecular components that can give rise to this dehydration resistance have not been identified.

The glycolipid trehalose 6,6′-dimycolate (TDM; cord factor) occurs in the outer envelope of all mycobacteria and is the most abundant extractable lipid at the surface of virulent MTb (14,15). (The recent discovery of TDM in *M. leprae*, the pathogen that causes leprosy, removed what had been the singular exception to its universal presence (16).) Since its isolation and identification as a toxic glycolipid half a century ago (5,17,18), the impact of TDM on organisms has been studied widely. TDM is known, for example, to be capable of inducing granulomas in animals; these granulomas are similar to those that are characteristic of tuberculosis infection (15,19). TDM also is capable of triggering increased chemokine and cytokine production (20), inhibiting trafficking of phagocytosed bacteria to acidic compartments in macrophages (21), and influencing the morphology of mycobacterial colonies (22–24). In liposomes, TDM inhibits vesicle fusion, potentially explaining its role in mediating the above-mentioned phagosome-lysosome fusion in vivo (25). The roles that TDM may play outside the host environment, however, and the advantages its presence may confer to pathogenic bacteria, remain poorly illuminated.

The glycan headgroup of TDM is trehalose (α-D-glucopyranosyl-(1,1)-α-D-glucopyranoside). This disaccharide is abundant in mycobacteria both as a free cytosolic component and in glycoconjugates at the cell envelope (26,27). Free trehalose is found in many microbes, fungi, and plants, where its preservation of membranes and proteins during freezing, osmotic stress, and dehydration is well known (28). Trehalose solutions also have been found to stabilize and preserve dry lipid bilayer membranes (29,30). Trehalose-containing glycolipids, however, are not common in nature. Given their manifestation in rugged mycobacteria and the above-mentioned properties of trehalose, we hypothesized that the presence of TDM may modulate membrane response during anhydrous stress.

We therefore designed two-dimensionally fluid, TDM-rich model membranes that mimic the structure of the mycobacterial envelope. We found that TDM imparts to membranes a striking resistance to desiccation; even membranes composed of a 1:3 molar ratio of glycolipid/phospholipids can be

Submitted November 9, 2007, and accepted for publication February 8, 2008.

Address reprint requests to Raghuveer Parthasarathy, E-mail: raghu@uoregon.edu.

Editor: Peter Hinterdorfer.

0006-3495/08/06/4718/07 $2.00

doi: 10.1529/biophysj.107.125542

dehydrated and rehydrated without significant loss of membrane integrity and functionality.

MATERIALS AND METHODS

Lipids

1,2-Dioleoyl-*sn*-glycero-3-phosphocholine (DOPC) was purchased from Avanti Polar Lipids (Alabaster, AL). Trehalose 6,6′-dimycolate was purchased from Sigma-Aldrich, St. Louis, MO (catalog no. T3034). Texas Red 1,2-dihexadecanoyl-*sn*-glycero-3-phosphoethanolamine (DHPE) was purchased from Invitrogen (Carlsbad, CA). The peak excitation and emission wavelengths for Texas Red are 583 and 601 nm, respectively.

Substrates

SiO_2/Si wafers were purchased from the UC Berkeley Microfabrication Laboratory, Berkeley, CA, and consisted of 54 nm thermal oxide on Si for experiments not involving fluorescence interference contrast microscopy (FLIC (see below)). The substrates were made hydrophobic by covalent linkage of octadecyltrichlorosilane (OTS) (Sigma-Aldrich) (31); in brief, wafers were cleaned in piranha solution (3:1 concentrated sulfuric acid/30% hydrogen peroxide), dried, and incubated 3 h in 3 mM OTS dissolved in toluene. After the incubation, the chips were rinsed in toluene and baked in air for 4 h at 100°C. The chips were then rinsed again with toluene. Hydrophobicity was verified by observing the contact angle of water droplets on representative substrates.

Monolayer deposition

Supported lipid monolayers were formed by Langmuir-Blodgett deposition techniques (32,33). In brief, a small chamber with 3 ml of phosphate-buffered saline (PBS), pH 7.4, was heated to the desired temperature with a temperature-controlled stage (QE-1; Warner Instruments, Hamden, CT). Lipid solutions of the desired composition then were mixed in chloroform and deposited on the surface of the PBS with a microsyringe to form a surfactant monolayer. The surface tension was continuously monitored by a tensiometer (Kibron Microtrough, Kibron instruments, Helsinki, Finland), which measured the capillary force acting on a metal surface probe. Lipids were added until the surface tension value saturated (typically between 35 and 50 mN/m, depending on composition), after which the monolayer was transferred to an OTS-coated SiO_2 /Si substrate by Langmuir-Blodgett deposition at 6mm/min, remaining in PBS buffer. At all stages of sample handling (monolayer preparation, transfer to substrates, rehydration, and imaging), the samples were maintained at 40°C ± 2°C.

Microscopy

Samples were examined and images obtained using an inverted fluorescence microscope (Nikon TE2000-E; Nikon, Tokyo, Japan) with a charged-coupled device camera (ORCA-ER; Hamamatsu, Hamamatsu City, Japan) and acquisition software (Nikon Elements; Nikon). Illumination was provided by a mercury arc lamp. Filter cubes purchased from Chroma Technology (Rockingham, VT) were used to examine the fluorescence from Texas Red (excitation band 530–580 nm; emission band 605–675 nm).

Monolayer dehydration/rehydration

Monolayer dehydration was achieved by removing PBS buffer with a pipette from the chamber housing the sample, followed by 1 min of drying under a flow of nitrogen gas. The chips then allowed to sit in open air for 10 min. Monolayer rehydration was achieved by submerging the chip facedown in clean PBS solution. Monolayers were allowed to equilibrate for 5 min before any images were taken.

Lipid mobility and fluorescence recovery after photobleaching

Monolayer mobility was measured by examining fluorescence recovery after photobleaching (FRAP). For each measurement, fluorescent probes in a region defined by a small aperture were bleached by intense illumination for 10 s. Images were acquired at discrete time points after bleaching. The local concentration C of molecules with unbleached fluorophores was proportional to the fluorescence intensity I. (The background intensity, due mainly to readout noise from the charge-coupled device camera, is measured and subtracted from each image. The density of fluorophores is low enough by more than an order of magnitude that nonlinear self-quenching effects are negligible. Thus, C is proportional to I.) Images were analyzed using custom-made software written in MATLAB (The MathWorks, Natick, MA). The diffusing molecules were assumed to obey the statistical relations governing two-dimensional random walks, and hence Fick's law: $D\ \nabla^2 C = \partial C/\partial t$, where t is time and D is the diffusion coefficient (34). To extract D from a pair of fluorescence images separated in time by an amount Δt, the initial intensity field was stepped forward for a series of time steps (∂t) by numerically implementing the spatial derivative ($\nabla^2 C$) as a difference equation accounting for first-, second- and third-nearest neighbors to evaluate the derivative at each image pixel. The ''diffused'' image was compared to the final observed intensity field at each step. The step number j that yielded the minimal mean-square deviation between the calculated and observed images gives the best fit value of D via the relation $D = j\ \Delta x^2/(2\Delta t)$, where Δx is the pixel size. (A simple one-dimensional illustration of this procedure can be found in Berg (34). Testing our algorithms on simulated diffusion images whose $C(x,t)$ functions could be analytically determined revealed a precision within 10% of the true values of D. The uncertainties for diffusion coefficients in our study are the standard errors of the mean of several ($N = 3$–16) measurements on multiple samples added in quadrature to an estimated 10% uncertainty in the FRAP analysis.

FLIC

FLIC experiments were performed on SiO_2/Si substrates microfabricated at the UC Berkeley Microfabrication Laboratory, Berkeley, CA, using standard photolithographic techniques to create repeating terraces of 16 oxide thicknesses spaced between 0 and 225 nm. The substrates were made hydrophobic with OTS, as described above. FLIC data, i.e., fluorescence images of supported monolayers on patterned substrates, were analyzed to extract the background-subtracted fluorescence intensities as a function of the various (measured) oxide thicknesses. Using custom software written in MATLAB to implement the optical principles inherent in FLIC, we related the measured intensity function to the fluorophore height, as described elsewhere (35,36).

Atomic force microscopy

Atomic force microscopy (AFM) was performed using an atomic force microscope (MFP 3D; Asylum Research, Santa Barbara, CA) in tapping mode with the cantilever and sample immersed in the aqueous buffer medium. Samples were prepared as described above (in PBS, and imaged at room temperature). The cantilevers used had a nominal spring constant of 5 N/m.

Nanosphere binding

Fluorescent neutravidin-conjugated nanospheres (diameter 0.04 μm) were purchased from Invitrogen. Biotinylated lipids (1,2-dipalmitoyl-*sn*-glycero-3-phosphoethanolamine-*N*-(cap Biotinyl)), denoted 16:0 Biotinyl cap-PE, were purchased from Avanti Polar Lipids. Supported monolayers of 88:(57-x):x:1 molar ratio TDM/DOPC/Biotinyl cap-PE/TR-DHPE with $x = 0$ or 1 were made, imaged, and dehydrated and rehydrated as detailed above. After rehydration, the supported monolayers were incubated for 10 min with 2 μl of 10^{-9} M neutravidin-conjugated beads, rinsed by immersion in clean PBS, and imaged using appropriate filter cubes.

Percolation calculations

The lattice-spanning probabilities $Q(p)$ were calculated by simulating the growth of percolation clusters on a 100 × 100 two-dimensional (2D) triangular lattice, implementing the recursive Leath algorithm (37) using custom software written in MATLAB. The Leath algorithm works as follows: A lattice site can be ''occupied'', ''unoccupied'', or ''unexamined.'' All sites of the lattice are initially designated as unexamined except for an initial occupied site. For a given value of the site occupancy probability p, the nearest neighbors of the occupied site are examined and identified as occupied, with probability p, or unoccupied, with probability $(1–p)$. All the unexamined neighbors of the newly occupied sites are then similarly examined. Recursively iterating this procedure reveals the growth of the cluster of occupied sites, which can either stop, if all neighbors are unoccupied sites, or continue until the boundaries of the lattice are reached. In our implementation, 1000 instances of the simulation were run for each value of p to determine the probability (Q) that the growing cluster would span the lattice, as opposed to ceasing growth before reaching the boundaries. In addition to the curves plotted in Fig. 3, the simulation returned the analytically known value $p_c = 0.5$, corroborating its accuracy.

RESULTS AND DISCUSSION

Supported membrane mimics of mycobacterial envelopes

We constructed an experimental model system that mimics the structure of the mycobacterial cell envelope. Outside the plasma membrane, a dense mycolic acid layer covalently linked to highly branched peptidoglycan and arabinogalactan strata comprises a hydrophobic, nonfluid substrate for the outermost, two-dimensionally fluid, glycolipid-rich monolayer; this outer monolayer is home to TDM and other noncovalently linked lipids (Fig. 1, *left*) (4,6,14,20,38–40). A supported membrane (33,41–43), in which a dense, hydrophobic, nonfluid OTS monolayer underlies a two-dimensionally fluid TDM-rich lipid monolayer, therefore recapitulates the essential envelope structure (Fig. 1, *right*). As detailed in Materials and Methods, the hydrophobic substrate is composed of a covalently bound self-assembled monolayer of OTS on SiO_2. The fluid lipid monolayer is formed by first assembling a monolayer of TDM plus fluorescent lipid probes (at most 1 mol % Texas Red DHPE) and DOPC phospholipids, in experiments on mixed membranes, at an air-water interface. This monolayer is then transferred to the hydrophobic substrate by Langmuir-Blodgett deposition (32), forming a solid-supported monolayer in an aqueous buffer. The fluorescent probes allow inspection by optical microscopy of membrane integrity and quantitative measurements of membrane fluidity measured via FRAP and topography measured via FLIC (see Materials and Methods).

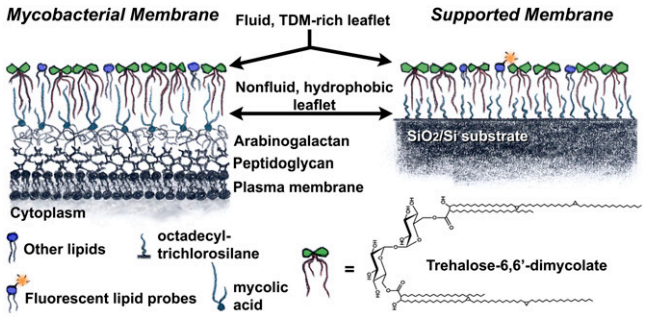

FIGURE 1 Schematic illustration of the mycobacterial envelope and our experimental supported membrane system. In both, the outermost leaflet is a two-dimensionally fluid lipid monolayer rich in the glycolipid TDM. Underlying this outer leaflet is a dense, hydrophobic, nonfluid monolayer composed in mycobacteria of mycolic acids covalently bound to the arabinogalactan layer underneath, and in our model platform of octadecyltrichlorosilane covalently bound to a silicon wafer.

TDM forms two-dimensionally fluid supported monolayers

TDM (with 1 mol % Texas Red DHPE present for visualization) forms two-dimensionally fluid supported monolayers at 40°C. Fluorescence microscopy shows uniform intensity fields characteristic of an intact membrane, and quantitative FRAP measurements demonstrate recovery of photobleached regions with a diffusion coefficient D of 1.26 ± 0.22 $\mu m^2/s$ (Fig. 2 *a*). At room temperature (22°C), TDM membranes are nonfluid and often show jagged features indicative of a gel or solid phase, consistent with calorimetric measurements of mycobacterial envelopes that find a fluidity transition temperature around 30–35°C (38,39).

We used FLIC (35,36,44,45) to verify the topographic structure of TDM-rich supported monolayers, providing corroboration that the structures formed were supported monolayers rather than larger structures, e.g., multilayers or aggregates of micelles. In FLIC, the presence of a reflective silicon substrate leads to optical interference of the excitation or emission light of a fluorophore with its reflection from the substrate (see Supplementary Material, Fig. S1 in Data S1). Especially by exploiting microfabricated substrates in which a series of SiO_2 thicknesses above the Si layer provides varying offsets for the interfering paths, fluorescence intensity can be related to fluorophore height with a precision of a few nanometers, as several studies have demonstrated in a variety of contexts (35,36,44–48). FLIC measurements of headgroup-conjugated Texas Red DHPE probes (1 mol %) in homogenous TDM membranes (see Materials and Methods) yielded heights of 2.7 ± 1.1 nm above the oxide surface, consistent with a monolayer structure. Images of membranes on FLIC substrates and measured intensity functions are provided in the Supplementary Material (Fig. S1 in Data S1).

We further verified the membrane topography using AFM (see Materials and Methods). In contrast to FLIC, AFM cannot provide absolute thickness measurements of an intact membrane; the AFM cantilever scans the surface, detecting differences in height. To image TDM membranes, we cooled samples from 35°C to room temperature (22°C) to create defects (holes). Regions of membrane appeared as plateaus above the exposed substrate with terrace heights of 2.7 nm, consistent with the value derived from FLIC. On the plateaus, the surface roughness was measured to be 0.15 nm (assessed

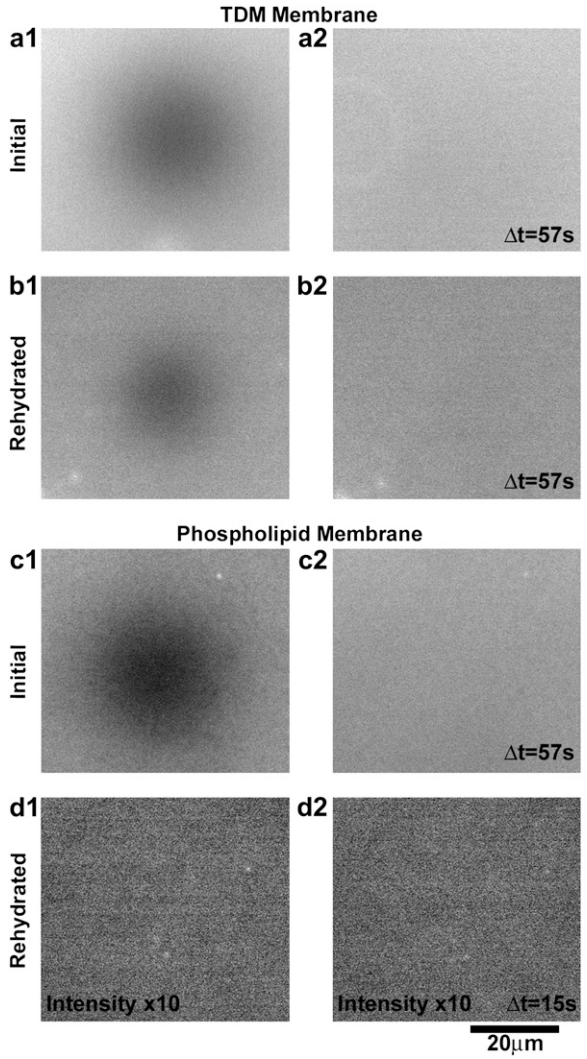

FIGURE 2 Membrane fluidity and desiccation resistance. (*a–d*) Fluorescence images of supported monolayers containing 1 mol % Texas Red DHPE. (*a1* and *a2*) Two images of a 99 mol % TDM monolayer after photobleaching a defined region, separated in time by $\Delta t = 57$ s, show recovery of a uniform intensity field, indicating fluidity. (*b1* and *b2*) FRAP images of a 99 mol % TDM monolayer after dehydration and subsequent rehydration also show fluorescence and recovery of the bleached pattern, indicating fluidity. (*c1* and *c2*) FRAP images of a 99 mol % DOPC monolayer similarly show an intact, fluid membrane. (*d1* and *d2*) After dehydration and rehydration, a 99 mol % DOPC monolayer shows negligible fluorescence beyond the background intensity and no measurable mobility, indicating an absence of lipids and a lack of survival during desiccation typical of phospholipids. The intensity in (*d*) has been enhanced by a factor of 10 with respect to that of (*c*).

as the standard deviation of the height over a typical 0.5 μm^2 region). AFM images and profiles across the plateau edges are provided in the Supplementary Material (Fig. S2 in Data S2).

TDM monolayers maintain integrity through dehydration and rehydration

The supported monolayers are dehydrated by removing them from their environment of PBS, drying with a stream of nitrogen gas for 1 min followed by exposure to ambient air for 10 min, and then rehydrated by immersion in PBS. After rehydration, the membranes again appear structurally uniform and, moreover, are mobile with diffusion coefficients comparable to their original values (1.01 ± 0.20 $\mu m^2/s$) (Fig. 2 *b*). In contrast, phospholipid membranes are well known to suffer irreparable structural damage on dehydration (29,30), and we verified this behavior. Initially intact, fluid DOPC membranes (with 1 mol % Texas Red DHPE) did not recover after dehydration and rehydration, showing little or no fluorescence signal, indicating an absence of lipids (Fig. 2, *c* and *d*). TDM displays a marked resilience with respect to desiccation.

TDM protects other membrane lipids from desiccation and preserves membrane functionality

To examine whether the dehydration resistance of TDM can extend to other lipids making up a membrane, we constructed mixed TDM/DOPC membranes (again with 1 mol % Texas Red DHPE). For all ratios of TDM/DOPC examined, ranging from 1:0 to 0:1, we were routinely able to form two-dimensionally fluid supported monolayers at 40°C (Fig. 3 *a*, *squares*). As the molar fraction of DOPC was increased in the range 0 to 75 mol %, the membrane diffusion coefficient rose from $D = 1.3$ to 4.5 $\mu m^2/s$, reflecting the greater mobility of DOPC compared to TDM. A peak in D around 25:75 TDM/DOPC may imply a structural transition in lipid packing, reminiscent of earlier reports examining molecular densities of TDM and other lipids at air-water interfaces (49). Dehydration and rehydration of these samples led to recovery—i.e., a uniform, bright fluorescence intensity and a measurable diffusion coefficient—in all samples ranging from 100 to 20 mol % TDM (Fig. 3 *a*, *triangles*). Membranes with lower fractions of TDM showed no discernible recovery. Plotting the ratio (D_R) of the measured D postrehydration to its initial value reveals a curve (Fig. 3 *b*) that shows near-complete recovery for TDM fractions down to 50%, decaying sharply to 0 around 15 mol %. Identifying the TDM fraction at which $D_R = 0.5$ as a characteristic density needed for recovery, we find that the presence of TDM down to mole fractions as low as 25% is sufficient to preserve a membrane during dehydration.

The fraction of recovered mobility (D_R) of the rehydrated membranes shows a sharp onset as a function of TDM fraction and a steep increase after the onset (Fig. 3 *b*)—features reminiscent of percolation transitions found in a wide variety of physical systems (50). In percolation problems, one considers, for example, a lattice in which each site is occupied with probability p and examines the probability Q that a connected cluster of occupied sites spans the lattice. Trivially, $Q(p = 0) = 0$ and $Q(p = 1) = 1$. For p between 0 and 1, however, $Q(p)$ has a less obvious form: Q is 0 for $0 \leq p \leq p_c$, and increases from 0 for $p > p_c$, where p_c is some (finite) critical probability. We suspected that the dependence of D_R

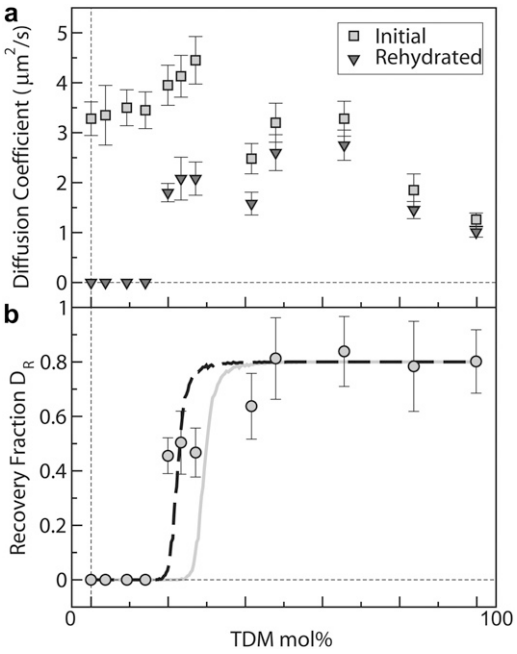

FIGURE 3 (*a*) Membrane diffusion coefficients, *D*, for TDM/DOPC–supported monolayers. Squares indicate data from prepared membranes, which show fluidity throughout the 0–100 mol % TDM range. Superimposed on this robust fluidity are additional trends: *D* increases with increasing DOPC fraction in the range 0–75 mol % DOPC and shows a small peak around 75 mol % DOPC that may indicate a packing transition. Triangles indicate diffusion coefficient values after dehydration and rehydration, which again demonstrate fluidity in the range 20–100 mol % TDM. In the range 0–15 mol %, TDM samples show no recovery as gauged by an absence of fluorescence intensity, and are therefore assigned a mobility of 0. (*b*) The ratio D_R of the membrane diffusion coefficient after dehydration and rehydration relative to its initial value (*circles*), show recovery over a large range of TDM concentration. The curves represent calculations from 2D percolation models with no adjustable parameters other than a saturation value of 0.8 (*gray line*), and with the ratio of the molecular areas of TDM and DOPC as a fit parameter (*dashed black line*).

on the TDM fraction indicates a percolation transition, with a geometric spanning of the membrane by TDM lipids determining its survival upon desiccation. We mapped Q onto D_R, treating the long-range mobility of fluorescent probes as a measure of connectivity. In general, analytic forms for $Q(p)$ do not exist, and so we simulated site-percolation on a 2D triangular lattice, similar in intermolecular coordination to a 2D fluid, to calculate $Q(p)$ (see Materials and Methods). If TDM and DOPC had the same molecular area, the TDM mole fraction (m) would simply equal the site probability, p. Because they do not, m and p are related by $m = p/[p + (1–p)r]$, where r is the ratio of the area per TDM molecule to that of DOPC, which follows from assigning to each TDM molecule r lattice sites rather than only 1. Because r is known experimentally to be > 1, and p_c in this 2D geometry is known to be 0.5, we expect a percolation transition at $m < 0.5$. In other words, the larger size of TDM enables it to form membrane-spanning clusters at concentrations < 50 mol %. The area per DOPC molecule is $A_{DOPC} = 0.71\ nm^2$ (51). The area per TDM is less certain, with values of $A_{TDM} = 1.87$, 1.35, and $1.60\ nm^2$ being reported in the literature (49,52,53). Using the mean value $A_{TDM} = 1.61\ nm^2$, from which $r = 2.26$, we calculated $Q(m)$ with no adjustable parameters other than the saturation value as $m \rightarrow 1$ being set to 0.8 to account for the imperfect recovery evident from the data. The resulting curve in is in good agreement with the measurements (Fig. 3 *b*, *gray*). Given the uncertainty in A_{TDM} and reports of TDM-induced compaction of molecular areas for mixed TDM-phospholipid monolayers (49), we also calculated $Q(m)$ with r adjusted to best fit the data, yielding $r = 3.24$ or $A_{TDM} = 2.30\ nm^2$ (Fig. 3 *b*, *black dashed line*). Both curves support the hypothesis that the percolation geometry of TDM determines the membrane's protection from desiccation.

The topography of mixed TDM/DOPC membranes was examined by FLIC, as described earlier, for TDM concentrations of 0, 50, 75, and 99 mol %, yielding fluorophore heights in the range 5 ± 4 nm with no systematic variation with TDM fraction. AFM measurements of 50 mol % TDM membranes were also attempted, but an absence of holes in the scanned regions precluded measurements of membrane thickness.

To investigate whether the ''network'' of TDM is preserving the functional integrity of the membrane as a whole and not only TDM lipids alone during dehydration and rehydration, we examined two separate indicators. The first was the presence and mobility of the fluorescent lipid probes used for imaging, which demonstrates their survival. Second, and most relevant for membrane function, we constructed TDM-rich lipid monolayers containing 1 mol % lipids with biotin-conjugated headgroups to examine the specific binding of neutravidin-conjugated nanospheres. After dehydration and rehydration, the membranes were incubated with nanospheres and unbound particles were removed by washing (see Materials and Methods). Fluorescence microscopy revealed the presence of the bound nanospheres at densities 300 × greater than control samples with no biotinylated lipids. The structures preserved by TDM were therefore capable of functional interactions with exogenous proteins. Images of fluorescent nanospheres bound to rehydrated TDM-rich membranes with and without biotinylated lipids are provided in the Supplementary Material (Fig. S3 in Data S3).

CONCLUSIONS

More than half a century ago, investigations of *M. tuberculosis* identified TDM as a major component of the mycobacterial envelope, comprising $\leq 2\%$ of the dry weight of MTb (5,17,18,54). Since then, a multitude of studies has explored the pathogenicity and molecular biology of MTb leading to the sequencing of its genome (55), for example. Also in the past few decades, researchers have illuminated the ability of free trehalose to preserve biomolecules from dehydration and other stresses in vitro and in a wide variety of organisms (28). The convergence of these two parallel tracks

of inquiry requires novel experimental methodologies in which biomimetic TDM-rich membranes are constructed and quantitatively probed with respect to mobility, topography, and specific biomolecular recognition. Devising and implementing this approach, we have discovered that TDM can form two-dimensionally fluid lipid monolayers that, unlike conventional lipid membranes, can maintain their integrity under anhydrous conditions. Strikingly, this protective capability extends to membranes in which TDM is present as a minority component, preserving the membrane structure and its functionality with respect to protein recognition.

Our observations provide the first reported case of dehydration resistance in a membrane provided by a membrane glycolipid, in contrast to extrinsic protective agents such as soluble sugars (30) or peripherally bound proteins (56). This finding may enable new approaches to membrane handling, fabrication, and manipulation that are incompatible with aqueous environments, enhancing the already considerable appeal of lipid membranes as biotechnological platforms.

In its biological context, we suggest that TDM may facilitate the survival of pathogenic bacteria like *M. tuberculosis* in dry environments that punctuate their residence in ''wet'' host organisms. Greater knowledge of the composition of mycobacterial membranes would further our understanding of the correlations between the biophysical properties of molecules like TDM and the biology of mycobacteria. The exact fraction of TDM in the cell envelope may vary considerably within strains of the same species, for example 0–53 wt. % in daughter strains of the *M. bovis* BCG strain (57), and its abundance is, in general, poorly quantified across species. Though recent mass spectrometry work has elucidated structural differences among lipids present in the cell envelope in detail (58), quantitative modern studies of lipid abundances are severely lacking. We hope that these findings spur such investigations.

We expect that the experimental platform developed here, in which a solid-supported, fluid monolayer mimics the structure and composition of the cell envelope, will continue to provide insight into mycobacterial biophysics beyond the surprising desiccation resistance uncovered by this study. It is important to note that, although the trehalose headgroup of TDM is likely to be the dominant determinant of anhydrous protection, the hydrophobic chains may also contribute via interactions with each other and with the underlying hydrophobic molecules (either the hydrophobic support in our experiments or the immobile hydrophobic leaflet in the mycobacterial envelope). We expect that synthetic modification of the glycolipid structure and the construction of alternate membrane geometries will delineate the various mechanisms that together provide protection from dehydration. In addition, membrane elaboration via incorporation of additional mycobacterial biomolecules, such as sulfolipids and different trehalose-containing glycolipids (59), will enable controlled, quantifiable investigations of the influence of these metabolites on bacterial membrane structure and behavior.

SUPPLEMENTARY MATERIAL

To view all of the supplemental files associated with this article, visit www.biophysj.org.

We thank Richard Castenholz and Michael Schelle for useful discussions; Jordan Crist for experimental assistance; and especially thank Ethan Minot and Tristan Deborde for performing atomic force microscopy on our behalf.

This work was supported by the National Institutes of Health (grant R01-AI51622 to C.R.B.), the Engineering and Technology Industry Council of Oregon (C.W.H.), and the Alfred P. Sloan Foundation (R.P.).

REFERENCES

1. Dye, C., S. Scheele, P. Dolin, V. Pathania, and M. C. Raviglione. 1999. Consensus statement. Global burden of tuberculosis: estimated incidence, prevalence, and mortality by country. WHO Global Surveillance and Monitoring Project. *JAMA*. 282:677–686.
2. Corbett, E. L., C. J. Watt, N. Walker, D. Maher, B. G. Williams, M. C. Raviglione, and C. Dye. 2003. The growing burden of tuberculosis: global trends and interactions with the HIV epidemic. *Arch. Intern. Med.* 163:1009–1021.
3. World Health Organization. Global tuberculosis control: surveillance, planning, financing. WHO report. 2007. World Health Organization, Geneva.
4. Barry 3rd, C. E., R. E. Lee, K. Mdluli, A. E. Sampson, B. G. Schroeder, R. A. Slayden, and Y. Yuan. 1998. Mycolic acids: structure, biosynthesis and physiological functions. *Prog. Lipid Res.* 37:143–179.
5. Asselineau, J. 1966. The Bacterial Lipids. Holden-Day, San Francisco, CA.
6. Brennan, P. J., and H. Nikaido. 1995. The envelope of mycobacteria. *Annu. Rev. Biochem.* 64:29–63.
7. Volk, W. A., D. C. Benjamin, R. J. Kadner, and J. T. Parsons. 1986. Essentials of Medical Microbiology. Lipincott, Philadelphia.
8. Van der Hoeden, J., editor. 1964. Zoonoses. Elsevier, New York.
9. Fraise, A., P. A. Lambert, and J.-Y. Maillard. 2004. Russell, Hugo & Ayliffe's Principles and Practice of Disinfection, Preservation & Sterilization. Wiley-Blackwell, New York.
10. Twitchell, D. C. 1905. The vitality of tubercle bacilli in sputum. *Trans. Nat. Assoc. for Study and Prevent. Tuberc. Ann. Meeting*. 221–230.
11. Soparker, M. B. 1917. The vitality of tubercle bacilli outside the body. *Indian J. Med. Res.* 4:627–650.
12. Smith, C. R. 1942. Survival of tubercle bacilli. *Am. Rev. Tuberc.* 45:334–345.
13. Desikan, K.V. and Sreevatsa. 1995. Extended studies on the viability of *Mycobacterium leprae* outside the human body. *Lepr. Rev.* 66:287–295.
14. Minnikin, D. E. 1982. Lipids: complex lipids, their chemistry, biosynthesis, and roles. *In* The Biology of the Mycobacteria. C. Ratledge and J. Stanford, editors. Academic Press, New York. 95–185.
15. Hunter, R. L., M. Olsen, C. Jagannath, and J. K. Actor. 2006. Trehalose 6,6′-dimycolate and lipid in the pathogenesis of caseating granulomas of tuberculosis in mice. *Am. J. Pathol.* 168:1249–1261.
16. Kai, M., Y. Fujita, Y. Maeda, N. Nakata, S. Izumi, I. Yano, and M. Makino. 2007. Identification of trehalose dimycolate (cord factor) in *Mycobacterium leprae*. *FEBS Lett.* 581:3345–3350.
17. Noll, H., and H. Bloch. 1953. A toxic lipid component of the tubercle bacillus (cord factor). II. Occurrence in chloroform extracts of young and older bacterial cultures. *Am. Rev. Tuberc.* 67:828–852.
18. Noll, H., and H. Bloch. 1955. Studies on the chemistry of the cord factor of *Mycobacterium tuberculosis*. *J. Biol. Chem.* 214:251–265.
19. Bekierkunst, A., I. S. Levij, E. Yarkoni, E. Vilkas, A. Adam, and E. Lederer. 1969. Granuloma formation induced in mice by chemically defined mycobacterial fractions. *J. Bacteriol.* 100:95–102.

20. Ryll, R., Y. Kumazawa, and I. Yano. 2001. Immunological properties of trehalose dimycolate (cord factor) and other mycolic acid-containing glycolipids a review. *Microbiol. Immunol.* 45:801–811.
21. Indrigo, J., R. L. Hunter Jr., and J. K. Actor. 2003. Cord factor trehalose 6,6′-dimycolate (TDM) mediates trafficking events during mycobacterial infection of murine macrophages. *Microbiology.* 149:2049–2059.
22. Hunter, R. L., N. Venkataprasad, and M. R. Olsen. 2006. The role of trehalose dimycolate (cord factor) on morphology of virulent *M. tuberculosis* in vitro. *Tuberculosis (Edinb.).* 86:349–356.
23. Glickman, M. S., J. S. Cox, and W. R. Jacobs Jr. 2000. A novel mycolic acid cyclopropane synthetase is required for cording, persistence, and virulence of *Mycobacterium tuberculosis*. *Mol. Cell.* 5:717–727.
24. Bloch, H. 1950. Studies on the virulence of tubercle bacilli; isolation and biological properties of a constituent of virulent organisms. *J. Exp. Med.* 91:197–218.
25. Spargo, B. J., L. M. Crowe, T. Ioneda, B. L. Beaman, and J. H. Crowe. 1991. Cord factor (alpha,alpha-trehalose 6,6′-dimycolate) inhibits fusion between phospholipid vesicles. *Proc. Natl. Acad. Sci. USA.* 88: 737–740.
26. Elbein, A. D., Y. T. Pan, I. Pastuszak, and D. Carroll. 2003. New insights on trehalose: a multifunctional molecule. *Glycobiology.* 13:17R–27R.
27. Elbein, A. D., and M. Mitchell. 1973. Levels of glycogen and trehalose in *Mycobacterium smegmatis* and the purification and properties of the glycogen synthetase. *J. Bacteriol.* 113:863–873.
28. Crowe, J. H., F. A. Hoekstra, and L. M. Crowe. 1992. Anhydrobiosis. *Annu. Rev. Physiol.* 54:579–599.
29. Crowe, J. H., L. M. Crowe, and D. Chapman. 1984. Preservation of membranes in anhydrobiotic organisms: the role of trehalose. *Science.* 223:701–703.
30. Albertorio, F., V. A. Chapa, X. Chen, A. J. Diaz, and P. S. Cremer. 2007. The alpha,alpha-(1→1) linkage of trehalose is key to anhydrobiotic preservation. *J. Am. Chem. Soc.* 129:10567–10574.
31. Maoz, R., and J. Sagiv. On the formation and structure of self-assembling monolayers. I. A comparative ATR-wettability study of Langmuir–Blodgett and adsorbed films on flat substrates and glass microbeads. *J. Colloid. Interface Sci.* 100:465–496.
32. Barnes, G., and I. Gentle. 2005. Interfacial Science: An Introduction. Oxford University Press, Oxford.
33. von Tscharner, V., and H. M. McConnell. 1981. Physical properties of lipid monolayers on alkylated planar glass surfaces. *Biophys. J.* 36: 421–427.
34. Berg, H. C. 1993. Random Walks in Biology. Princeton University Press, Princeton, NJ.
35. Parthasarathy, R., and J. T. Groves. 2004. Optical techniques for imaging membrane topography. *Cell Biochem. Biophys.* 41:391–414.
36. Groves, J. T., R. Parthasarathy, and M. B. Forstner. 2007. Imaging of membrane dynamics. *Annu. Rev. Biomed. Eng.* In press
37. Leath, P. L. 1976. Cluster size and boundary distribution near percolation threshold. *Phys. Rev. B.* 14:5046–5055.
38. Liu, J., E. Y. Rosenberg, and H. Nikaido. 1995. Fluidity of the lipid domain of cell wall from *Mycobacterium chelonae*. *Proc. Natl. Acad. Sci. USA.* 92:11254–11258.
39. Liu, J., H. E. Takiff, and H. Nikaido. 1996. Active efflux of fluoroquinolones in *Mycobacterium smegmatis* mediated by LfrA, a multidrug efflux pump. *J. Bacteriol.* 178:3791–3795.
40. Dmitriev, B. A., S. Ehlers, E. T. Rietschel, and P. J. Brennan. 2000. Molecular mechanics of the mycobacterial cell wall: from horizontal layers to vertical scaffolds. *Int. J. Med. Microbiol.* 290:251–258.
41. Kuhl, T. L., J. Majewski, J. Y. Wong, S. Steinberg, D. E. Leckband, J. N. Israelachvili, and G. S. Smith. 1998. A neutron reflectivity study of polymer-modified phospholipid monolayers at the solid-solution interface: polyethylene glycol-lipids on silane-modified substrates. *Biophys. J.* 75:2352–2362.
42. Sanii, B., and A. N. Parikh. 2007. Surface-energy dependent spreading of lipid monolayers and bilayers. *Soft Matter.* 3:974–977.
43. Stottrup, B. L., S. L. Veatch, and S. L. Keller. 2004. Nonequilibrium behavior in supported lipid membranes containing cholesterol. *Biophys. J.* 86:2942–2950.
44. Lambacher, A., and P. Fromherz. 1996. Fluorescence interference-contrast microscopy on oxidized silicon using a monomolecular dye layer. *Appl. Phys. A.* 63:207–216.
45. Lambacher, A., and P. Fromherz. 2002. Luminescence of dye molecules on oxidized silicon and fluorescence interference contrast microscopy of biomembranes. *J. Opt. Soc. Am. B.* 19:1435–1453.
46. Kerssemakers, J., J. Howard, H. Hess, and S. Diez. 2006. The distance that kinesin-1 holds its cargo from the microtubule surface measured by fluorescence interference contrast microscopy. *Proc. Natl. Acad. Sci. USA.* 103:15812–15817.
47. Kiessling, V., and L. K. Tamm. 2003. Measuring distances in supported bilayers by fluorescence interference-contrast microscopy: polymer supports and SNARE proteins. *Biophys. J.* 84:408–418.
48. Kaizuka, Y., and J. T. Groves. 2006. Hydrodynamic damping of membrane thermal fluctuations near surfaces imaged by fluorescence interference microscopy. *Phys. Rev. Lett.* 96:118101.
49. Almog, R., and C. A. Mannella. 1996. Molecular packing of cord factor and its interaction with phosphatidylinositol in mixed monolayers. *Biophys. J.* 71:3311–3319.
50. Sahimi, M. 1994. Applications of Percolation Theory. Taylor & Francis, Bristol, PA.
51. Costigan, S. C., P. J. Booth, and R. H. Templer. 2000. Estimations of lipid bilayer geometry in fluid lamellar phases. *Biochim. Biophys. Acta.* 1468:41–54.
52. Retzinger, G. S., S. C. Meredith, K. Takayama, R. L. Hunter, and F. J. Kezdy. 1981. The role of surface in the biological activities of trehalose 6,6′-dimycolate. Surface properties and development of a model system. *J. Biol. Chem.* 256:8208–8216.
53. Crowe, L. M., B. J. Spargo, T. Ioneda, B. L. Beaman, and J. H. Crowe. 1994. Interaction of cord factor (alpha, alpha′-trehalose-6,6′-dimycolate) with phospholipids. *Biochim. Biophys. Acta.* 1194:53–60.
54. Noll, H. 1956. The chemistry of cord factor, a toxic glycolipid of *M. tuberculosis*. *Bibl. Tuberc.* 10:149–183.
55. Cole, S. T., R. Brosch, J. Parkhill, T. Garnier, C. Churcher, D. Harris, S. V. Gordon, K. Eiglmeier, S. Gas, C. E. Barry 3rd, F. Tekaia, K. Badcock, et al. 1998. Deciphering the biology of *Mycobacterium tuberculosis* from the complete genome sequence. *Nature.* 393:537–544.
56. Holden, M. A., S. Y. Jung, T. Yang, E. T. Castellana, and P. S. Cremer. 2004. Creating fluid and air-stable solid supported lipid bilayers. *J. Am. Chem. Soc.* 126:6512–6513.
57. Asselineau, J. and V. Portelance. 1974. Comparative study of the free lipids of eight BCG daughter strains. *Recent Res. Cancer. Res.* 47:214–220.
58. Fujita, Y., T. Naka, M. R. McNeil, and I. Yano. 2005. Intact molecular characterization of cord factor (trehalose 6,6′-dimycolate) from nine species of mycobacteria by MALDI-TOF mass spectrometry. *Microbiology.* 151:3403–3416.
59. Schelle, M. W., and C. R. Bertozzi. 2006. Sulfate metabolism in mycobacteria. *ChemBioChem.* 7:1516–1524.